Università di Catania

DOTTORATO DI RICERCA IN

BASIC AND APPLIED BIOMEDICAL SCIENCES

(XXXVIII CICLO)

Coordinatore:

Prof. Massimo Libra

Antioxidant system remodeling underlies off-target effects of anti-BCMA-Targeted Immunotherapy in Multiple Myeloma

Dottorando

Dott. Enrico La Spina

Supervisor: Chiar.mo Prof. Daniele Tibullo

ANNO ACCADEMICO

2025-2026

INTRODUCTION

1. Multiple Myeloma

1.2 Pathophysiology of Multiple Myeloma

Multiple myeloma (MM) is a haematological malignancy characterized by terminally differentiated Plasma Cells (PCs) inside bone marrow (BM), immunosuppression and end-organ damage (1). The disease is usually associated with the production of a monoclonal immunoglobulin fragment, commonly referred to as M-protein, secreted by the clonal PCs (2). Clinical manifestations arise both from the accumulation of malignant PCs and from soluble mediators released by these cells, such as cytokines and growth factors. The most frequent organ-related complications include hypercalcemia, renal dysfunction, anemia, and osteolytic lesions or fractures. Collectively, these hallmarks are designated as the CRAB features, which define symptomatic MM and guide treatment decisions (3). These are:

- **Calcaemia**: it occurs in approximately 30% of patients; widespread bone destruction induced by tumor is the primary cause of the hypercalcemia (4);
- **Renal insufficiency**: this complication is present in 20 – 40% of patients; the main causes of renal failure are the accumulation of monoclonal light chains in distal and collecting renal tubules and hypercalcemia (5);
- **Anaemia**: it is diagnosed in 73% of patients and it is a consequence to the suppression of erythropoiesis by cytokine (6);
- **Bone disease**: it shows as lytic lesions or osteopenia and is usually combined with severe pain, pathological fracture, spinal cord compression, vertebral collapse; osteolytic bone disease is a consequence of bone homeostasis perturbation, which is physiologically regulated by osteoblasts and osteoclasts (7);

Myeloma evolves from an asymptomatic pre-malignant stage of PCs proliferation termed monoclonal gammopathy of undetermined clinical significance (usually known as MGUS) that may progress to an intermediate but more advanced pre-malignant stage defined smouldering myeloma (SMM) and, finally, to symptomatic myeloma (8).MM exists along a biological and clinical continuum that encompasses precursor states. The earliest and most common is

monoclonal gammopathy of undetermined significance (MGUS), which is characterized by low levels of BM infiltration by clonal PCs and the presence of a monoclonal protein in the serum, but without end-organ damage. MGUS is asymptomatic but carries a small annual risk of progression to overt MM. An intermediate state, known as smoldering multiple myeloma (SMM), is defined by higher plasma cell burden and M-protein levels than MGUS, yet still lacks CRAB features. Both MGUS and SMM precede symptomatic MM and illustrate the stepwise transformation from indolent to aggressive PC malignancy (9). The pathogenesis of MM is intricately linked to B-cell development and PCs differentiation (10).

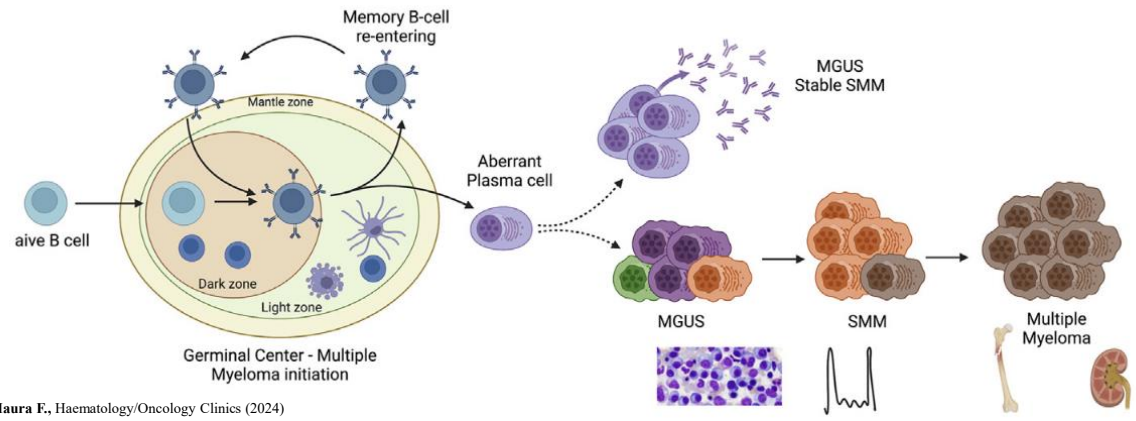

Figure 1 Initiation of PCs neoplasms in the germinal center. The initial genetics events (chromosome translocations and hyperdiploidy) occur in the germinal center B-cell and are present in all stages of plasma cell neoplasms. Subsequent genetic events cause the progression from MGUS to SMM. Figure was generated using biorender.

Hematopoietic stem cells in the BM give rise to immature B lymphocytes, which undergo V(D)J recombination to generate a highly diverse immunoglobulin repertoire. Once B cells reach secondary lymphoid organs such as the spleen and lymph nodes, they undergo additional processes including somatic hypermutation, affinity maturation, and immunoglobulin class-switch recombination. These modifications enable the production of antibodies with increased antigen specificity and diverse effector functions (11). However, such processes involve the generation of DNA double-strand breaks, which under normal conditions are tightly regulated. If repair mechanisms fail, aberrant recombination events may occur, leading to chromosomal translocations or other structural genomic alterations. Certain translocations provide growth advantages to B cells and are thought to represent initiating events in plasma cell dyscrasias (12). For example, the t(11;14)(q13;q32) translocation, observed in approximately 14% of MM patients, juxtaposes the immunoglobulin heavy-chain locus to the CCND1 gene, resulting in cyclin D1 overexpression and deregulated cell-cycle progression (13). Other recurrent cytogenetic abnormalities in MM include deletion of 1p, gain of 1q, deletion of 13q, and

deletion of 17p, each of which contributes to disease heterogeneity and impacts prognosis (14). Beyond chromosomal alterations, epigenetic deregulations, some patients display relatively indolent disease with long periods of stability, while others present with aggressive features and rapid progression (15). Understanding the molecular mechanisms behind these differences is critical for improving patient stratification and for developing more precise therapeutic interventions. The molecular changes, together with microenvironmental factors within the BM niche, collectively promote survival, proliferation and drug resistance (DR) of clonal PCs. Thus, MM represents a complex disorder where genetic, epigenetic, and signaling pathway alterations converge to generate a malignancy with diverse clinical presentations and outcomes (16).

1.3 Current treatment strategies and future directions for MM

At the beginning of the 21st century, the median overall survival of patients with MM was approximately three years (17). Over the past two decades, survival outcomes have significantly improved, largely due to the introduction of novel therapeutic agents, including proteasome inhibitors (PIs), immunomodulatory drugs (IMiDs), and monoclonal antibodies (mAbs) (18).

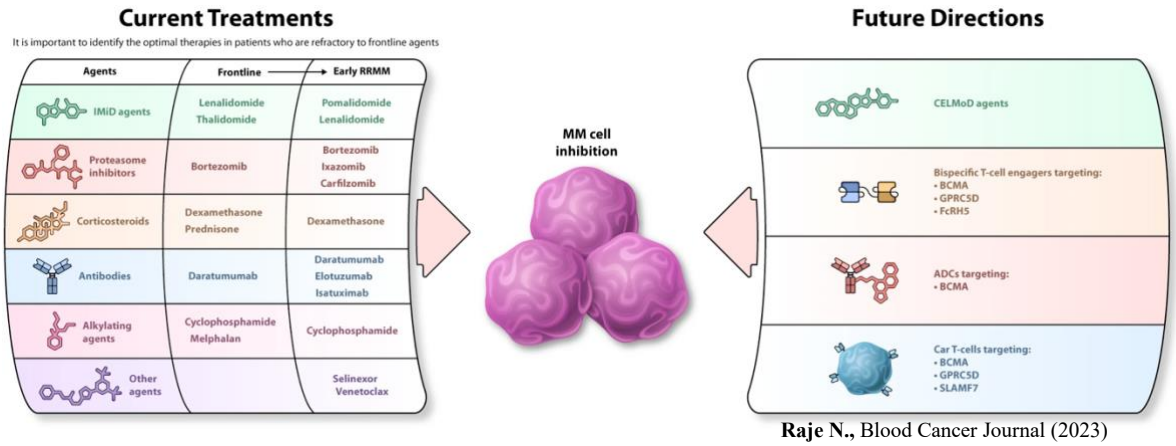

Figure 2. Overview of current and emerging treatment strategies for RRMM. Agents currently used in frontline and relapsed/refractory settings are shown on the left, while therapies under clinical investigation or entering clinical use are listed on the right. *Abbreviations:* ADC, antibody–drug conjugate; BCMA, B-cell maturation antigen; CAR, chimeric antigen receptor; CELMoD, cereblon E3 ligase modulating drug; FcRH5, Fc receptor–homolog 5; GPRC5D, G protein–coupled receptor family C group 5; mAb, monoclonal antibody; MM, multiple myeloma; SLAMF7, signaling lymphocytic activation molecule family member 7.

1.3.1 Proteasome inhibitors (PIs).

Among the milestones in MM therapy are PIs, a class that includes Bortezomib (BTZ), the second-generation agent carfilzomib, and the first oral PI, ixazomib (19). BTZ, a boronic acid

dipeptide, was the first selective and reversible inhibitor of the 26S proteasome, a multi-subunit complex responsible for the degradation of regulatory proteins involved in cell-cycle control, transcriptional regulation, and apoptosis. Malignant PCs are particularly vulnerable to proteasome blockade due to their constitutive production of large quantities of immunoglobulins, which imposes stress on the endoplasmic reticulum and activates the unfolded protein response. By impairing protein degradation, BTZ induces accumulation of misfolded proteins, mitochondrial depolarization, and apoptosis. Additional mechanisms include inhibition of NF-κB signaling, activation of c-Jun N-terminal kinase, and stabilization of cell-cycle inhibitors, collectively leading to growth arrest and cytotoxicity in myeloma cells. Despite the remarkable progress achieved with these agents, MM remains largely incurable, mainly due to the ability of malignant PCs to develop DR (20).

1.3.2 Immunomodulatory drugs (IMiDs),

A second therapeutic class is represented by IMiDs, including thalidomide and its next-generation analogues lenalidomide and pomalidomide. These agents exhibit pleiotropic anti-myeloma activity by modulating immune effector functions, exerting anti-angiogenic and anti-inflammatory effects, and directly inhibiting proliferation of PCs. Their combination with PIs has become the backbone of modern treatment regimens, significantly improving depth of response (21).

1.3.3 Monoclonal antibodies (mAbs)

Surface antigen CD38 is expressed on the malignant PCs of patients with MM (22) and the mAb daratumumab was the first anti-CD38 approach to be approved by the FDA for relapsed/refractory MM (RRMM) (23). Daratumumab causes cell death through different mechanisms including complement-dependent and antibody-dependent cell-mediated cytotoxicity, antibody-dependent cellular phagocytosis, and apoptosis (24). Elotuzumab, the second monoclonal antibody approved for treatment of MM, targets SLAMF7, activating antibody cell-mediated cytotoxicity, enhancing the cytotoxicity of NK cells, and inhibiting the interaction of myeloma cell with bone marrow stromal cells (25). In addition, autologous stem cell transplantation (ASCT) remains an effective consolidation strategy for eligible patients, typically administered after induction regimens incorporating combinations of PIs, IMiDs, alkylating agents, corticosteroids, and more recently Drug-conjugated mAbs (ADCs) (26).

1.3.4 mAbs drug-conjugates

Antibody–drug conjugates (ADCs) are an innovative class of anticancer agents that integrate the target specificity of monoclonal antibodies with the cytotoxic potency of small-molecule chemotherapeutics. This dual nature enables selective delivery of highly active compounds to malignant cells while limiting systemic exposure and off-target toxicity. The clinical efficacy of ADCs depends not only on the choice of antibody and cytotoxic payload but also on intracellular trafficking, processing, and controlled release of the drug within tumor cells, which collectively determine the induction of cell death (27). Structurally, an ADC consists of three fundamental components: (1) the monoclonal antibody, which provides antigen specificity; (2) the cytotoxic payload, often far more potent than conventional chemotherapeutics; and (3) the linker, which connects the two while ensuring stability in circulation and efficient drug release within the target cell. A critical design challenge lies in balancing linker stability in plasma with its lability in the lysosomal environment, where proteolytic cleavage or pH-sensitive hydrolysis allows liberation of the active drug. Among the earliest payloads explored were synthetic analogues of dolastatin-10, a cytotoxic peptide of marine origin (28). Compounds such as auristatin E (AE) and monomethyl auristatin F (MMAF) were successfully conjugated to chimeric monoclonal antibodies including cBR96, which targets the Lewis Y antigen expressed on several carcinomas, and cAC10, directed against CD30, a well-established marker in hematologic malignancies (29). These prototypes demonstrated that conjugation of auristatins to tumor-specific antibodies, through optimized linker chemistry, allowed stable circulation and selective internalization. Upon lysosomal degradation of the antibody–linker complex, the cytotoxic payload was efficiently released inside antigen-positive (Ag^+) cells, leading to microtubule disruption, mitotic arrest, and apoptosis (30)

1.3.4.1 Belantamab-Mafodotin (BeMa)

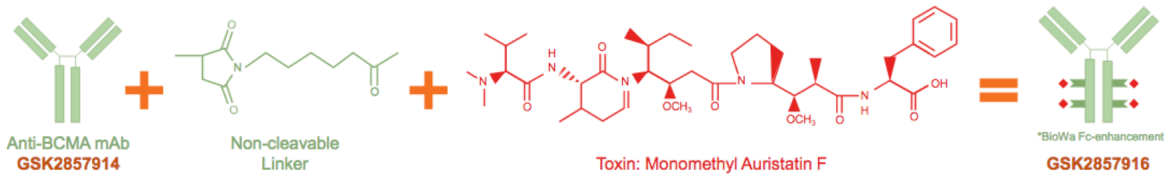

Figure 3. Belantamab-mafodotin or GSK2857916 is a humanized, afucosylated, IgG1 anti-BCMA monoclonal antibody (belantamab or GSK2857914) conjugated to monomethyl auristatin-F (MMAF). The drug is being investigated in the treatment of patients with for the treatment of patients with for the treatment of patients with multiple myeloma. The drug linker technology is licensed from Seattle Genetics and the monoclonal antibody is produced using POTELLIGENT Technology licensed from BioWa. Image courtesy GSK.

One of the most promising areas of innovation is targeted immunotherapy against B-cell maturation antigen (BCMA). BCMA (TNFRSF17) is a transmembrane receptor of the tumor necrosis factor receptor family, selectively expressed during late B-cell differentiation and highly upregulated on malignant PCs, while being absent or minimally expressed on naïve B cells, memory B cells, $CD34^{+}$ hematopoietic progenitors, and most healthy tissues (31). This restricted expression profile makes BCMA an attractive therapeutic target. Among the anti-BCMA strategies, Belantamab-Mafodotin (BeMa) is a first-in-class ADC approved for the treatment of tetra-RRMMpatients. BeMa consists of a humanized anti-BCMA mAb conjugated via stable linkers to MMAF. Although its principal mechanisms of action involve internalization, lysosomal degradation, and targeted release of MMAF into $BCMA^{+}$ cells, additional immunological effects, such as antibody-dependent cytotoxicity, may also contribute. From DREAMM-2 clinical trial, almost 30% of patients became refractory and nearly, 50% of MM patients receiving BeMa experience ophthalmologic side effects at corneal level by dose four, more specifically lipid keratopathy (LK) (including superficial punctate keratopathy) and/or microcyst-like epithelial changes (MECs), are the most common events (72% of patients). These are mostly due to off-target delivery and deconjugation of the MMAF which may give rise to the well-characterized “bystander effect” in which a small fraction of the cytotoxic payload is prematurely cleaved from its linker and may act towards healthy surrounding cells (32). Cogan and Kuwabara (33) proposed that most patients with LK shows high circulating cholesterol levels within lipoproteins (34), (35) and several clinical studies indicate that the lipid content of lipoproteins is the most prevalent biomarker of MM progression. (36).

1.4 Mechanisms of Pharmacological Resistance in Multiple Myeloma

1.4.1 Fatty acid cell composition

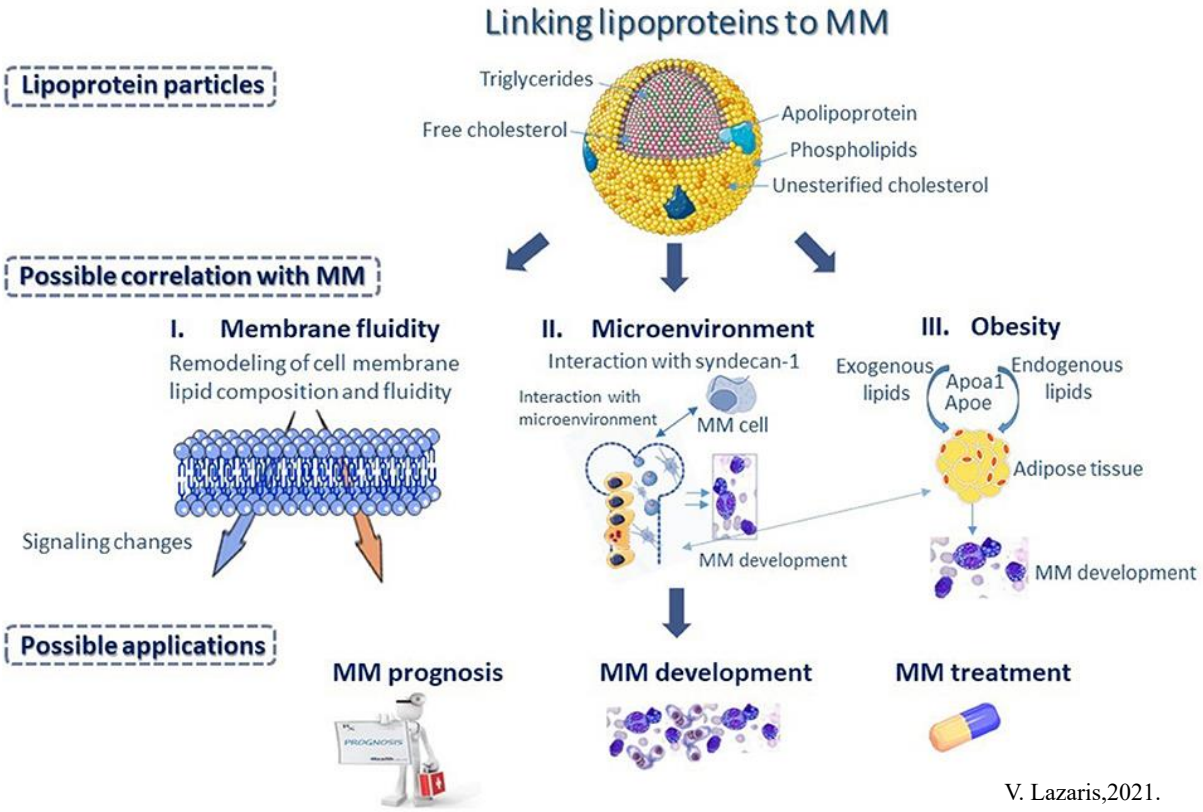

Figure 4. Variations in apolipoprotein/lipid composition across lipoprotein classes may serve as biomarkers linking lipoproteins to MM. Dysregulated lipoprotein metabolism can (I) alter MM cell membrane fluidity and signaling, (II) remodel the b one-marrow niche via syndecan-1, and (III) promote adipogenesis and obesity that support MM progression. APOA1 and APOE are plausible mediators of these effects.

High-density lipoprotein (HDL), one of the five major classes of circulating lipoproteins, plays a crucial role in lipid homeostasis. HDL are primarily involved in the reverse transport of cholesterol and the redistribution of lipids from peripheral tissues, thereby regulating membrane composition and cellular energy balance (37). Lipids carried by HDL may be utilized as an energy source through β-oxidation, or alternatively stored within the cytoplasm in the form of cytoplasmic lipid droplets LDs (38).The aberrant accumulation of LDs has emerged as a hallmark of progression, metabolic adaptation, and DR (39). LDs not only serve as reservoirs for neutral lipids such as triglycerides and cholesteryl esters but also provide metabolic flexibility, enabling malignant cells to counteract environmental stressors, nutrient deprivation, and drug-induced stress. When free fatty acids (FFAs) and cholesteryl esters are delivered from lipoproteins into the intracellular compartment, they can fuel the biogenesis of LDs, which in turn give rise to a wide spectrum of lipid species. These bioactive lipid families participate in membrane biosynthesis, energy storage, intracellular signaling, and modulation

of apoptosis pathways (40). Thus, the remodeling of lipid composition is not a passive consequence of altered metabolism but rather a regulated process that provides tumor cells with a selective advantage. Fatty acids differ in carbon chain length and in the number and position of double bonds. Based on their degree of unsaturation, they are broadly classified into saturated fatty acids (SFAs), monounsaturated fatty acids (MUFAs), and polyunsaturated fatty acids (PUFAs) (41). In cancer cells, these subgroups exhibit distinct functional roles. For instance, palmitic acid (PA), a major saturated fatty acid, is an essential precursor for MUFAs synthesis. Through the enzymatic activity of stearoyl-CoA desaturase-1 (SCD1), PA can be converted into palmitoleic acid, thereby contributing to an increased pool of MUFAs within the tumor cell membrane. Elevated MUFAs levels have been correlated with enhanced membrane fluidity, signaling plasticity, and resistance to lipid peroxidation. The MUFAs/PUFAs ratio represent a critical determinant of cancer cell fate. MUFAs confer protection against oxidative stress by reducing the availability of peroxidation susceptible substrates (42). Conversely, PUFAs, with multiple double bonds, are more susceptible to oxidation and can act as mediators of ferroptotic cell death when not adequately counterbalanced by antioxidant defenses. By increasing MUFAs synthesis and elevating the MUFA/PUFA ratio, cancer cells effectively protect themselves from oxidative damage, sustain redox balance, and minimize ROS-induced oxidative stress(43).

1.4.2 Oxidative stress

The emergence of DR represents a major limitation in the treatment of MM, and several biological mechanisms have been proposed to explain this phenomenon. One important aspect is the deregulation of the redox homeostasis in malignant PCs. Unlike normal cells, MM cells maintain persistently elevated levels of reactive oxygen species (ROS), which activate adaptive stress-response pathways and allow them to tolerate oxidative pressure while preserving cellular viability (44). This chronic exposure to oxidative stress results in the upregulation of antioxidant defense systems, thereby reducing the cytotoxic impact of therapies that rely on ROS accumulation as a mechanism of tumor cell killing. Consequently, the enhanced ROS-scavenging machinery not only protects myeloma cells from oxidative damage but also attenuates the efficacy of ROS-inducing chemotherapeutic agents. Among the different antioxidant systems mobilized to counterbalance oxidative stress, a pivotal role is played by glutathione peroxidase 4 (GPx4). GPx4 is a unique intracellular enzyme capable of suppressing lipid peroxidation within cellular membranes, thereby preserving membrane integrity and

preventing ferroptotic cell death (45). By neutralizing lipid-derived ROS, GPx4 not only protects MM cells from oxidative damage but also interferes with drug-induced cytotoxic pathways, further contributing to resistance. Taken together, these findings highlight that MM cells exploit redox adaptation mechanisms to survive under hostile conditions created both by their intrinsic biology and by therapeutic pressure. A deeper understanding of these pathways, particularly the role of ROS metabolism and antioxidant enzymes such as GPx4, is essential for the design of next-generation therapeutic strategies aimed at overcoming resistance and improving the durability of treatment responses in multiple myeloma (46).

1.5 Aim of the study

Integrating proteomic, lipidomic, and in vitro functional assays, this study aims to define the molecular response of MM cells to BeMa and to provide a comprehensive framework for its mechanism of action.

2 Material and methods

2.1 Cell culture and treatments

Myeloma cell lines (U266, NCI-H929, and OPM2) were cultured in RPMI 1640 medium supplemented with 10% fetal bovine serum (FBS) and 1% penicillin/streptomycin at 37 °C in a humidified atmosphere containing 5% CO_2. Cells were treated with increasing concentrations of BeMa obtained from GlaxoSmithKline (GSK, Brentford, UK) ranging from 1 to 100 µg/mL for up to 72 hours to generate cell viability dose–response curves. The concentration of 50 µg/mL, corresponding to the clinically relevant dose, was selected for subsequent analyses, including cell viability assays at 48 hours. the 24-hour treatment time point was used to evaluate early drug effects as lipidomic profiling, and for mechanistic and functional experiments. RSL3 (Cat. No. S8155; Selleck Chemicals, Houston, TX, USA) and N-acetylcysteine (NAC) (Cat. No. A7250; Sigma-Aldrich, St. Louis, MO, USA) were used in selected experiments to modulate oxidative stress and glutathione metabolism.

2.2 Palmitic acid supplementation

Palmitic acid (PA, C16:0; Cayman Chemical, Cat# 10006627) from a 100 mmol/L stock solution was freshly diluted in 10% BSA (Sigma-Aldrich, Cat# A4612). A 2.5 mmol/L PA solution was then further diluted to 125 µmol/L in pre-warmed RPMI medium (37 °C). Equal amounts of BSA were added to control cells in each experiment, and lower PA concentrations

were diluted in 1% BSA to standardize the BSA content across all conditions. The BeMa-sensitive multiple myeloma cell lines U266 and NCI-H929 were maintained in culture with fresh PA (125 µM) + 1% BSA for 7 days, with supplementation renewed at each medium replacement

2.3 Oil-Red-O staining

After incubation with BeMa (50 µg/mL), 3 × 10^6 HMCLs were washed with PBS and fixed with 4% paraformaldehyde for 10 min at room temperature. Cells were then stained with 1% Oil Red O solution prepared from Oil Red O powder (Sigma-Aldrich, Cat# O0625) dissolved in isopropanol and filtered before use (0.22 µm filter). For the working solution, three parts of the 1% Oil Red O stock were mixed with two parts of distilled water, allowed to stand for 10 min, and filtered again immediately before staining. Cells were incubated with the freshly prepared working solution for 10 min, followed by nuclear counterstaining with DAPI (1 µg/mL) for 30 min at room temperature.

2.4 Flow cytometry

For apoptosis evaluation, 5x10^5 cells were washed and resuspended in 100 µL of PBS. 1 µL of Annexin V-FITC solution and 1 µl of PI (Beckmam Coulter) were added to cell suspension and mixed gently. Cells were incubated for 15 min in the dark. Finally, 400 µl of 1X binding buffer was added and cell preparation was analyzed by flow cytometry (MACSQuant Analyzer 10, Miltenyi Biotec). To evaluate BCMA expression in all cell lines, they were washed and resuspended in 100 µl of PBS. 10 µl of anti-BCMA-PE (Beckman Coulter), was added to each tube. Cells were incubated for 15 min at room temperature, protected from light. After centrifugation, cells were washed in 1 ml of PBS and analyzed using flow cytometer. To determine lipidROS sensor and neutral cytoplasmatic lipids, were used C11-BODIPY$^{581/591}$ (#D3861) and BODIPY$^{493/503}$ (#D3922), (Invitrogen, USA), respectively. The day before the experiment, 1x10^5 cells (for U266 and NCI-H929) or 0,8X10^5 (for OPM2) per well were seeded in 96-well plates and treated with BeMa 50µg/mL. The day of the experiment, cells were and resuspended in 500 µL 1× phosphate-buffered solution (PBS) containing 2 µM C11-BODIPY$^{581/591}$ and incubated for 30 min at 37 °C in a cell culture incubator. Cells were centrifuged at 1400 rpm/min at room temperature for 5 min, the supernatants were removed, resuspended in 500 µL of fresh 1× PBS, and analysed using a flow cytometer (MACSQuant Analyzer 10,

Miltenyi Biotec) equipped with a 488 nm laser for excitation. The same procedure was esecuted for BODIPY$^{493/503}$. Data were collected from the FL1 channel (527 nm). A minimum of 10x10^5 cells were analysed per condition.

2.5 HPLC Analysis of Reduced Glutathione (GSH)

Intracellular GSH levels analyses were performed on a Surveyor HPLC system equipped with a photodiode array detector (Thermo Fisher Scientific Italia, Rodano, Milan, Italy). Separation was achieved on a Hypersil C18 column (250 × 4.6 mm, 5 µm) using an isocratic mobile phase containing 12 mM tetrabutylammonium hydroxide, 10 mM KH_2PO_4, and 0.125% methanol, adjusted to pH 7.0. The flow rate was set to 1.2 mL/min, and the column temperature maintained at 10 °C. Detection was performed at 206 nm, and GSH concentrations were determined by comparing peak areas with standard calibration curves prepared from ultrapure GSH solutions.

2.6 Proteomic

Samples of peripheral blood (PB) from male and female patients affected by multiple myeloma were grouped based on disease stage: Outset, refractory and relapse. Control samples were also analyzed by using the same experimental conditions. For metabolomic analysis, the extraction was conducted by adding 4 volumes of a cold solution of ACN/MeOH (1:1 v/v) to each sample. The supernatants were recovered by centrifuging at 12,000 rpm for 10 min. The samples were dried under vacuum and suspended in an aqueous solution containing 5 mM ammonium formate acidified with 0.2% formic acid for the LC-MRM/MS analysis.

2.6.1 Liquid Chromatography–Mass Spectrometry (LC–MS) analysis

Serum samples were subjected to a comprehensive proteomic workflow integrating both discovery and targeted mass spectrometry approaches. In the discovery phase, peptide mixtures were separated by nano-liquid chromatography and analyzed by tandem mass spectrometry (LC–MS/MS) on an LTQ Orbitrap XL system (Thermo Fisher) operating in data-dependent acquisition (DDA) mode to identify differentially abundant proteins. For the targeted phase, selected peptides were quantified by liquid chromatography coupled to a triple quadrupole/linear ion trap mass spectrometer (LC–MRM/MS, 5500 QTRAP, AB Sciex) operating in multiple reaction monitoring (MRM) mode. Chromatographic separations were performed on C18 columns under optimized gradients. This combined approach enabled both

broad protein profiling and accurate quantification of selected targets, providing a robust characterization of serum proteomic changes associated with BeMa treatment.

2.6.2 In solution digestion

For proteomics analysis, 10 µL of 84 sample from all the patients were subjected to a in solution digestion protocol. The samples diluted with denaturing buffer (6M Urea, 25 mM AMBIC) were treated with 20 mM DTT and incubated at 60 °C for 1 hour. After cooling the samples, the reduced cysteines were alkylated with 40 mM IAM and incubated in the dark for 1 hour at room temperature. A solution of 20 mM DTT was added to the protein mixture for 1 hour at room temperature to quench the alkylation process. A solution of trypsin (1 µg/µL) was added to each sample in a 1:50 of enzyme:substrate ratio. The enzymatic hydrolysis was performed for 15 h at 37°C in a thermostatic bath. Each sample was treated with the same desalting procedure using stage tips containing three layers of 3M Empore C18 membrane. Stage tips were washed with 100 µL 0.1% formic acid and peptides were recovered with a double step of elution: 50 µL of 50% acetonitrile and, subsequently, with 80% acetonitrile, both acidified with 0.2% formic acid. The peptide mixture was dried in a vacuum Speed-Vac, and re-suspended in 200 µL 2% acetonitrile, 0.5% formic acid and analysed by LC-MS/MS apparatus.

2.6.4 Data processing

Raw data files were processed by using MaxQuant software (1.6.8.0 version) (Tyanova, S., Temu, T., Carlson, A., Sinitcyn, P., Mann, M. and Cox, J., Visualization of LC-MS/MS proteomics data in MaxQuant, Proteomics, 2015, 15, pp 1453–1456). The following parameters were used for raw data processing: trypsin enzyme specificity, 3 missed tryptic cleavages, oxidation of methionine and pyroGlu from Gln as variable modifications and cysteine (C) carbamidomethylation as a fixed modification. Identification parameters included minimum peptide length of 6 amino acids, minimum of 1 peptide (both razor and unique peptide). Peptide tolerance of 10 ppm, fragment mass tolerance of ± 0.02 Da. All proteins were filtered according to a false discovery rate (FDR) of 0.01% applied both at peptide and protein levels and a maximum peptide posterior error probability (PEP) of 1. The derived peak list generated by Quant.exe (the first part of MaxQuant) was searched using the Andromeda search engine integrated into the MaxQuant against the specific fasta file of Homo sapiens obtained from the UNIPROT web site. MaxQuant output files were subsequently processed using Perseus (version 1.6.8.0) (Tyanova, S., Temu, T., Sinitcyn, P., Carlson, A., Hein, M., Geiger,

T., Mann, M. and Cox, J. The Perseus computational platform for comprehensive analysis of (prote)omics data. Nature Methods, 2016) software platforms. An experimental design template was used to get merged replicate experiments (each data set contained two technical replicates) into a single column containing all the proteins into every sample. Contaminants, reverse, and only identified by site hits were filtered out. Expression values of LFQ intensity were log2 transformed and only the protein rows containing a minimum of 2 valid values were maintained within Perseus matrix. Missing values were replaced by random numbers drawn from a normal distribution with a width of 0.3 and a down shift of 1.8. The complete list of proteins included UniProt id, gene name, protein name, score, and sequence coverage % (Supplementary material table SX).

2.7 qRT-PCR analysis

Total RNA was extracted from cells using Trizol reagent and quantified using a UV spectrophotometer (NANODROP 1000, Thermofisher). One microgram of total RNA (in 20 µL reaction volume) was reverse-transcribed in cDNA using reverse-transcriptase (Applied Biosystem) and oligo-dT primers in a standard reaction. The quantitative real-time polymerase chain reaction (qRT-PCR) of the resultant cDNA was performed using Sybr Green PCR Master Mix (ThermoFisher Scientific) and 7900HT Fast Real-Time PCR System (Thermo Fisher). Expression of the following human genes was evaluated: ACSL4 (FW: GCTATCTCCTCAGACACACCGA, RW: AGGTGCTCCAACTCTGCCAGTA); GPx4(FW: ACAAGAACGGCTGCGTGGTGAA, RW: GCCACACACTTGTGGAGCTAGA); SLC7A11 (FW: ATGCAGTGGCAGTGACCTTT, RW: GGCAACAAAGATCGGAACTG); B2M (Fw: AGCAGCATCATGGAGGTTTG; Rw: AGCCCTCCTAGAGCTACCTG); GAPDH (Fw: AATGGGCAGCCGTTAGGAAA; Rw: GCCCAATACGACCAAATCAGAG).

2.8 Statistical analysis

All statistics were performed using GraphPad Prism (version 10.00 for Mac, GraphPad Software, San Diego, CA, USA). Data that passed normality test were statistical analyzed using Student's t-test or ANOVA test where appropriate. A p- value < 0.05 was considered to indicate a statistically significant difference between experimental and control groups.

3 Results

3.1 Serum from RRMM patients shows an increase in apolipoproteins involved in lipid transport

To investigate systemic protein alterations associated with multiple myeloma and to identify circulating biomarkers linked to disease progression and treatment response, a label-free quantitative proteomic analysis was performed on serum samples from patients and healthy donors. Serum was selected as it captures both tumor-derived and host-related metabolic and inflammatory changes, providing a comprehensive picture of the systemic impact of the disease and its treatment. Fourteen serum samples — 8 from healthy donors (HD), 5 from newly diagnosed MM (NDMM), and 5 from relapsed/refractory MM (RRMM) — were subjected to enzymatic digestion and analyzed by LC–MS/MS. Hierarchical clustering revealed a clear distinction between HD and MM samples, while NDMM and RRMM displayed partial overlap (Fig. 5A). Proteins were classified as upregulated (fold change > 1.2) or downregulated (< 0.9). Compared with HD, NDMM samples showed 53% upregulated and 24% downregulated proteins, whereas RRMM displayed 29% and 34%, respectively (Fig. 5B). Statistical analysis identified 27 significantly dysregulated proteins in NDMM and 47 in RRMM compared to HD (Supplementary Tables 1 and 2). STRING network analysis (Fig. 5C) highlighted functional interactions among these proteins, while Reactome enrichment (Fig. 5D) revealed that upregulated proteins in RRMM were mainly involved in lipoprotein remodeling, fat-soluble vitamin metabolism, and plasma lipoprotein assembly, whereas downregulated ones were associated with hemostasis and platelet degranulation. Notably, increased levels of apolipoproteins A1, A2, and C2 — key HDL components responsible for triglyceride hydrolysis and lipid homeostasis — have been previously correlated with improved overall and progression-free survival in MM patients (47).

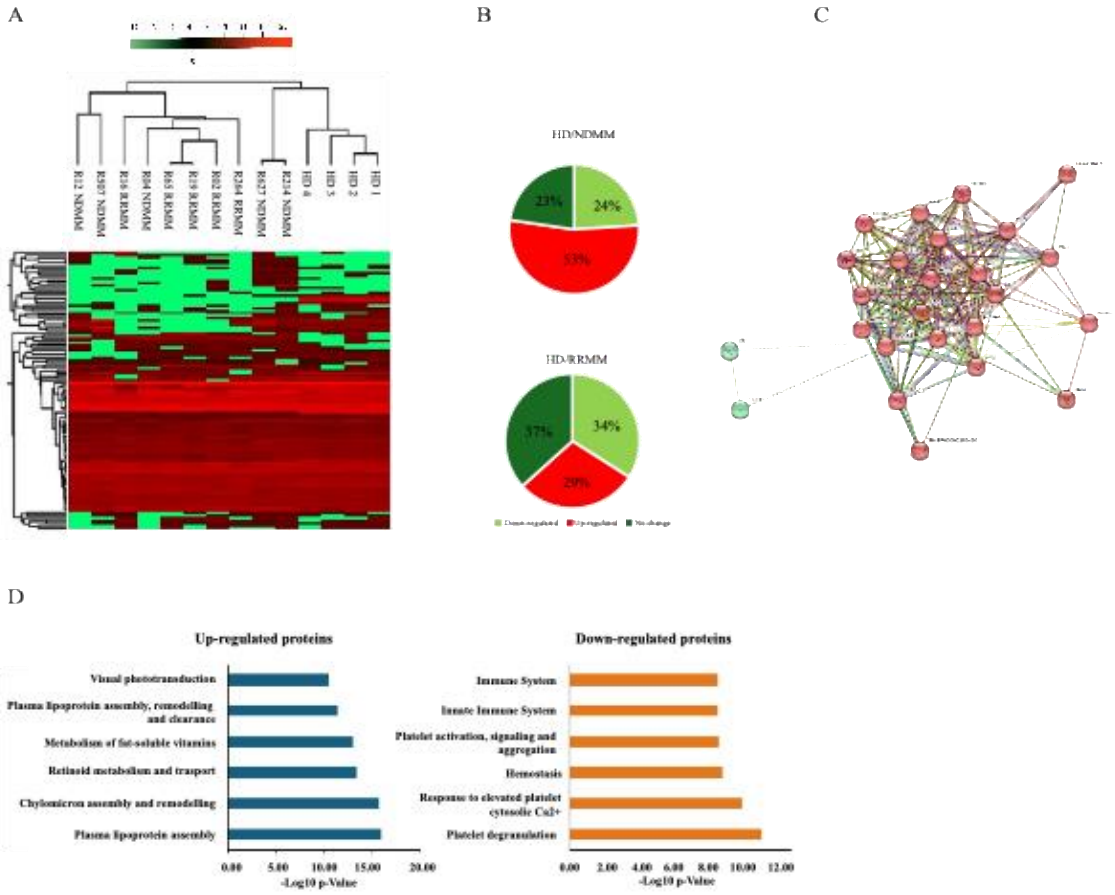

Figure 5. Serum from RRMM patients shows an increase in apolipoproteins involved in lipid transport. (A) Heatmap clustering of spectral data from newly diagnosed NDMM, RRMM, and HD. (B) Venn diagram of differentially expressed proteins. (C) STRING network analysis of the most significantly altered proteins. (D) Gene ontology (GO) analysis of the 12 most enriched biological pathways.

3.2 BeMa triggers lipid remodeling and cell death pathways that promote drug susceptibility

Consistently with proteomic evidence of altered lipid handling in RRMM patients, it was investigated whether these metabolic features influence cellular response to BeMa. Despite comparable BCMA expression levels in all MM cell lines, a dose-dependent reduction in cell viability was observed in U266 and NCI-H929 cells, but not in OPM2 cells. Based on the dose–response analysis (Supplementary Fig. 1), the concentration of 50 µg/mL BeMa, corresponding to the clinically relevant dose, was selected for subsequent experiments (Fig. 6A). Moreover, following 48-hour exposure to 50 µg/mL BeMa, FACS analysis revealed G2/M arrest in U266 and NCI-H929, while OPM2 cells displayed no perturbation (Fig. 6B). Interestingly, the intracellular distribution of neutral lipids was assessed by Oil Red O staining in U266 and OPM2 cells following BeMa treatment (50 µg/mL, 48 h). In U266 cells, BeMa exposure led to

a marked reduction in LDs compared with untreated controls. Quantitative analysis confirmed a decrease in total LD area percentage. Conversely, OPM2 cells exhibited a significant accumulation of LDs upon BeMa treatment, as evidenced by an increased LDs area percentage (Fig. 6C). This led us to hypothesize that MM cells modulate intracellular lipids availability to overcome stress BeMa-induced. Supporting this, long-term culturing U266 cells with 125 μM palmitic acid (PA) conjugated to BSA resulted in restored viability after BeMa exposure, compared to controls (Fig. 6D).

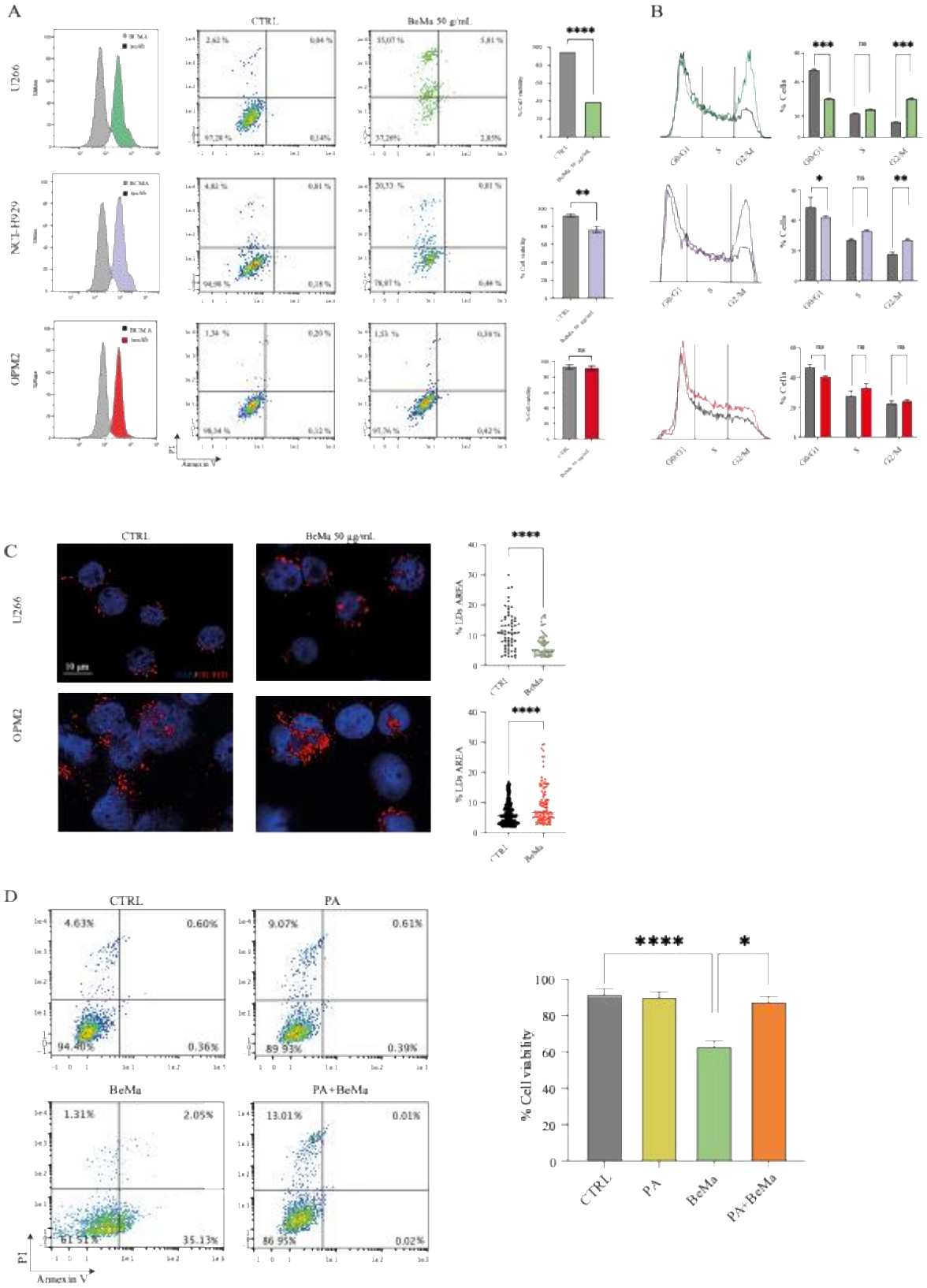

Figure 6. BeMa in vitro induces cell death and LDs modulation enhancing drug susceptibility. (A) MM cells were incubated with BeMa (50 µg/mL) or vehicle for 48 h, stained with annexin V-FITC/PI, and analyzed by flow cytometry. (B) Cell-cycle analysis after 48 h treatment with BeMa or vehicle using propidium iodide staining. (C) Oil Red O staining and ImageJ-based quantification of LDs in U266 and OPM2 cells treated with BeMa for 24 h, showing changes in LD area, average size, and number. (D) Cell viability of U266 and NCI-H929 cells after exogenous PA exposure and BeMa treatment. Data are presented as mean ± SD. *p < 0.05, **p < 0.01, ***p < 0.001, ****p < 0.0001, ns = not significant.

3.3 BeMa treatment induces lipid peroxidation and MUFA:PUFA remodeling

Recent studies have shown that elevated levels of MUFA suppress ferroptosis, a form of regulated cell death driven by peroxidation of PUFA which are hallmark of ferroptosis (48). As shown in Fig. 7A, BeMa exposure led to a significant increase in lipid peroxidation in the sensitive U266 and NCI-H929 cell lines, whereas no oxidation was observed in OPM2 cells. Consistently, comprehensive quantitative lipidomic profiling revealed that U266 cells, upon BeMa treatment, displayed a significant decrease in the MUFA/PUFA ratio, indicating a relative depletion of MUFA—particularly oleic acid (C18:1) — and enrichment in PUFA species, such as stearidonic acid (DHA, C22:6 n-3). NCI-H929 cells displayed no significant modulation of this ratio following BeMa treatment. In contrast, OPM2 cells exhibited a significant increase in the MUFA/PUFA ratio following BeMa treatment, reflecting an enrichment in MUFA—particularly oleic acid (C18:1) — and a concomitant reduction in PUFA species, notably arachidonic acid (C20:4 n-6) (Fig. 7B). Consistent with our previous studies showing that MM cells respond to BTZ-induced ROS by activating antioxidant-related genes as a compensatory mechanism (48) we investigated the expression levels of ferroptosis-related genes at baseline. Surprisingly, OPM2 cells displayed transcriptional ACSL4 down-regulation, a key enzyme involved in PUFA biosynthesis together with a robust antioxidant defense, characterized by elevated expression of SLC7A11 and GPX4, along with extracellular GSH levels up to 8-fold higher than in U266 cells (Fig. 7C).

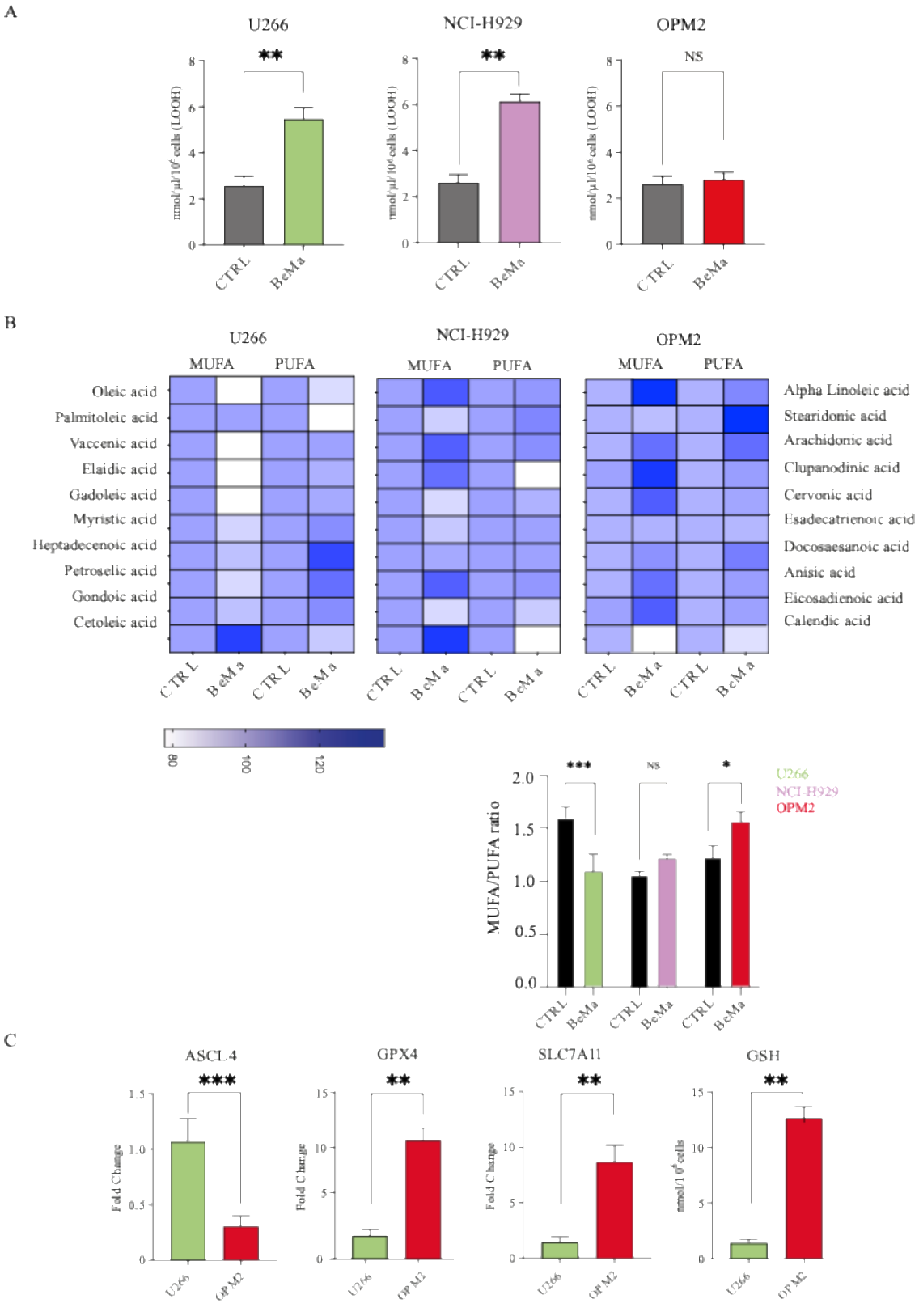

Figure 7. **MUFA:PUFA imbalance and GPx4-dependent redox defense induces oxidative stress sensitivity to anti-BCMA targeted therapy**. (A) Lipid peroxidation measured by BODIPY 581/591 C11 staining and flow cytometry in MM cells treated with BeMa (50 µg/mL). (B) Heatmap showing relative abundance of lipid species measured by UPLC-MS/MS after BeMa treatment. (C) Basal mRNA expression of ACSL4, GPx4, and SLC7A11 in U266 and OPM2 cells. GSH basal intracellular concentrations were measured by HPLC. Data are expressed as fold change over control. Statistical analysis: two-tailed unpaired Student's t test; *p < 0.05, **p < 0.01, ***p < 0.001.

3.4. Pharmacological GPx4 inhibition sensitize OPM2 to ferroptosis

To assess the contribution of oxidative stress–related pathways to BeMa susceptibility, OPM2 cells were exposed to the GPX4 inhibitor RSL3, either alone or in combination with BeMa. FACS analysis revealed that RSL3 treatment increased the proportion of PI-positive cells compared with control, while co-treatment with BeMa and RSL3 further enhanced cell death percentages at 24 h (Fig. 8A). Kinetic analysis of lipid ROS generation showed a time-dependent rise following RSL3 exposure, detectable as early as 3 h and peaking at 6 h post-treatment (Fig. 8B). The combination of BeMa and RSL3 produced the highest levels of lipid ROS at all time points compared with single treatments. In parallel, the antioxidant response was evaluated by supplementing cells with N-acetylcysteine (NAC), a GSH precursor. As shown in Fig. 8C, NAC pre-treatment markedly reduced lipid peroxidation levels and restored cell viability in both BeMa- and RSL3-treated cells, with the most pronounced effect observed in the BeMa + RSL3 co-treatment group.

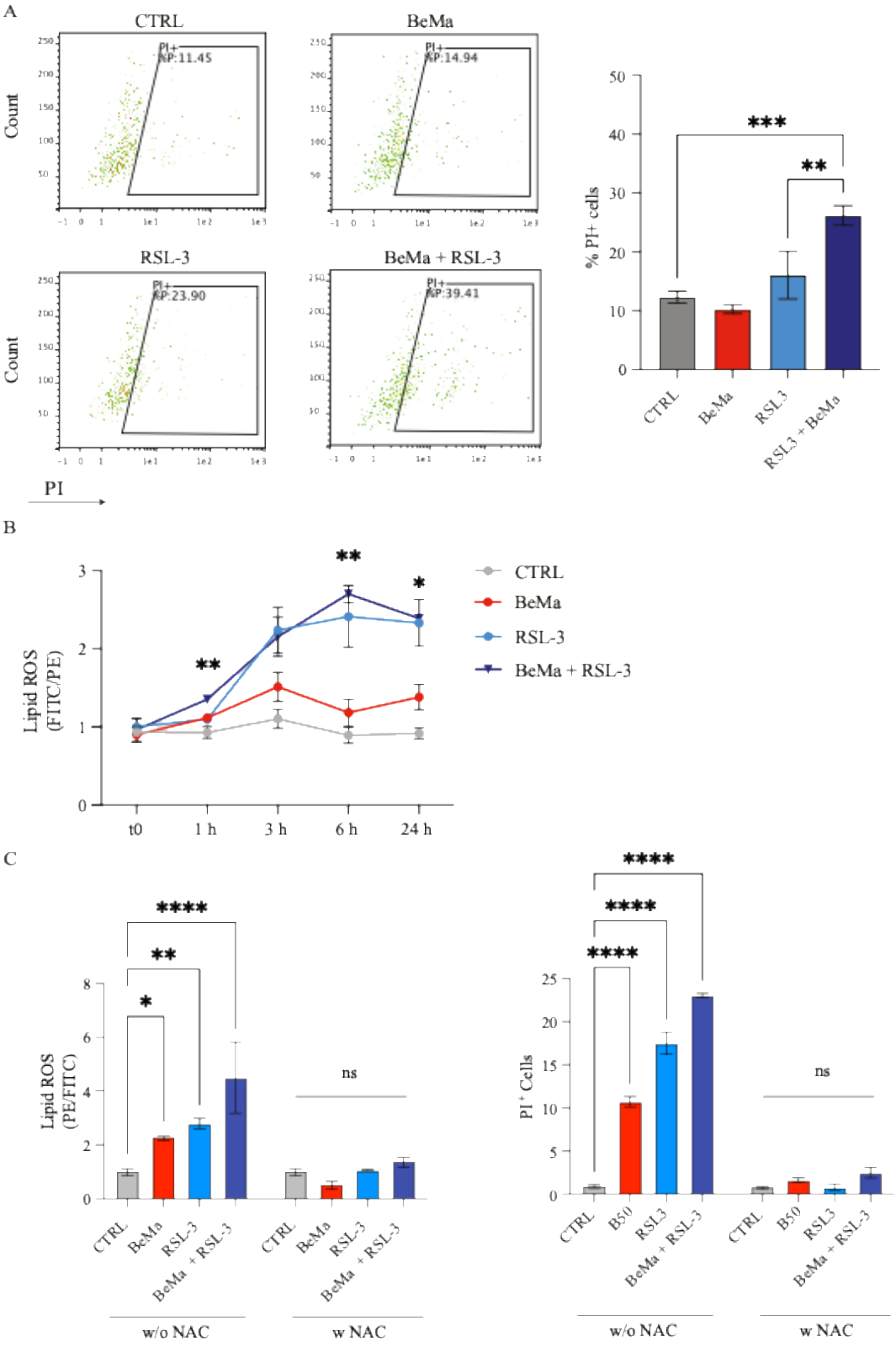

Figure 8. Pharmacological GPx4 inhibition sensitize OPM2 to Ferroptosis. (A) Percentage of PI^+ cells after 24 h exposure to BeMa (50 µg/mL), RSL-3 (0.5 µM), or their combination. (B) Lipid ROS production assessed over time by FITC/PE ratio (median fluorescence intensity) in cells treated with BeMa, RSL-3, or both. Data are expressed as MFI ± SEM. (C) Evaluation of antioxidant protection by N-acetylcysteine (NAC, 1 mM) pre-treatment for 24 h. NAC supplementation reduced lipid ROS and PI positivity in cells treated with BeMa, RSL3, or their combination compared with untreated controls. Data are presented as mean ± SD from three independent experiments; $p < 0.05$ was considered significant.

4. Discussion

In line with the pivotal DREAMM-2 study demonstrating that BeMa inhibits microtubule spindle formation during the G2/M phase of $BCMA^+$ cells (49), our findings confirm that BeMa exposure leads to cell cycle arrest in U266 and NCI-H929 cells, whereas OPM2 cells remain unaffected. Importantly, recent DREAMM-3 and DREAMM-6 clinical studies have reported that BeMa monotherapy, while effective in a subset of patients, often encounters resistance, thus reinforcing the translational relevance of our mechanistic observations (48) (50). The lack of correlation between BeMa sensitivity and BCMA surface expression prompted us to focus on the resistant OPM2 cytotype to elucidate alternative resistance mechanisms. MM-PCs differ from their healthy counterparts in part due to their distinct lipidomic profile (51). Proteomic analysis of RRMM patient sera compared with HD revealed a significant overexpression of apolipoproteins, including APO-A1, APO-A2, and APO-C2. APO-A1, a major component of HDL particles and cofactor for lecithin–cholesterol acyltransferase (LCAT), plays a crucial role in cholesteryl ester formation, whereas APO-C2 participates in triglyceride hydrolysis, releasing free fatty acids essential for cellular homeostasis. Elevated expression of these apolipoproteins may reflect an adaptive metabolic state in MM cells that enhances lipid utilization to sustain survival and proliferation (52). In the bone marrow microenvironment, adipocytes account for up to 70% of marrow volume and serve as a key lipid source for MM cell (53). These adipocytes release palmitic acid (PA) into the extracellular space, fueling metabolic reprogramming toward lipid oxidation and biosynthesis. Once internalized, PA contributes to membrane formation, energy storage, and signaling cascades that collectively promote tumor growth (54). This lipid dependency, although beneficial for tumor fitness, may also represent a potential therapeutic vulnerability in RRMM. Interestingly, lipid accumulation has been reported among the major adverse effects of BeMa, particularly in corneal epithelial cells(55), further linking BeMa exposure to altered lipid handling. Together, these data suggest that the equilibrium between lipid storage and utilization may critically modulate BeMa sensitivity. Our in vitro findings reinforce this concept. OPM2 cells, despite their resistance to BeMa, displayed increased accumulation of LDs following treatment, while sensitive U266 and NCI-H929 cells exhibited a reduction in LDs content. These observations suggest that resistant cells may use LDs formation as a buffering system to sequester excess lipids and protect against drug-induced oxidative stress. Increasing evidence supports the notion that LDs are not inert reservoirs but active metabolic hubs regulating lipid trafficking, signaling, and stress responses (56). Recent studies in acute myeloid leukemia and breast cancer have

demonstrated that LD accumulation provides a source of MUFAs that can be mobilized to counteract oxidative damage and ferroptotic cell death (57). Ferroptosis is an iron-dependent, non-apoptotic form of regulated cell death characterized by the accumulation of lipid peroxides, mainly derived from PUFAs within cellular membranes (58). In many cancers, cells rely on strong antioxidant systems to limit ROS production and maintain redox equilibrium (59–61). However, when antioxidant capacity is overwhelmed, excessive PUFA peroxidation occurs, leading to membrane rupture and cell death (43). The interplay between lipid composition and redox homeostasis is therefore a critical determinant of therapy-induced oxidative stress and drug sensitivity (62,63). Key enzymes govern the ferroptotic process. The acyl-CoA synthetase long-chain family member 4 (ACSL4) promotes incorporation of PUFAs into phospholipids, sensitizing cells to peroxidation (64,65). In parallel, the glutathione peroxidase 4 (GPX4)–glutathione (GSH) axis serves as a primary defense against lipid peroxide accumulation by reducing phospholipid hydroperoxides using GSH as an electron donor (46,66,67). Ferroptosis inducers (FINs) under investigation exploit this axis by either depleting GSH through cystine import inhibition (type I FINs, e.g., erastin) or by directly inhibiting GPX4 (type II FINs, e.g., RSL3) (68). Consistent with these mechanisms, we observed that BeMa-sensitive U266 and NCI-H929 cells exhibited elevated lipid ROS upon drug exposure, consistent with increased PUFA oxidation and decreased expression of GPX4 and SLC7A11, together with high basal levels of ACSL4—features indicative of a ferroptosis-prone phenotype. In contrast, OPM2 cells maintained redox stability through enhanced MUFA biosynthesis and elevated GPX4, SLC7A11, and GSH levels. Lipidomic profiling further confirmed a higher MUFA/PUFA ratio in OPM2, driven by increased oleic acid (C18:1) and reduced arachidonic acid (C20:4 n-6). These findings support the notion that lipid remodeling toward MUFA enrichment underlies ferroptosis resistance and attenuates oxidative lipid damage following BeMa exposure. The tumor microenvironment further reinforces this resistance (69). BM stromal cells, macrophages, and adipocytes secrete antioxidants and lipids that buffer malignant plasma cells from oxidative injury (70). Tumor-associated macrophages (TAMs), for instance, release cysteine and GSH, sustaining GPX4-dependent detoxification pathways (71). Thus, ferroptosis resistance in MM cannot be attributed solely to intrinsic cellular mechanisms but must be viewed within the broader context of metabolic support from the microenvironment. From a translational standpoint, our findings suggest potential therapeutic strategies. Combining BeMa with ferroptosis inducers such as RSL3, or with SCD1 inhibitors to reduce MUFA biosynthesis, may restore ferroptotic susceptibility and overcome drug resistance. Conversely, modulation of the antioxidant network with agents like N-

acetylcysteine (NAC) may paradoxically protect against excessive oxidative stress, providing a valuable tool to predict patient response. Taken together, our results demonstrate that oxidative stress plays a central role in BeMa response and that resistance in MM plasma cells is mediated by precise lipid remodeling aimed at minimizing peroxidation. These insights reveal a critical link between lipid metabolism, redox regulation, and therapeutic outcome, offering a rationale for integrating ferroptosis-targeting agents into clinical regimens. Targeting lipid desaturation and antioxidant pathways, either alone or in combination with anti-BCMA therapies, may pave the way for more effective and durable responses in relapsed or refractory multiple myeloma.

5. References

1. Kumar SK, Rajkumar V, Kyle RA, van Duin M, Sonneveld P, Mateos MV, et al. Multiple myeloma. Nat Rev Dis Primer. 2017 July 20;3:17046.

2. Abduh MS. An overview of multiple myeloma: A monoclonal plasma cell malignancy's diagnosis, management, and treatment modalities. Saudi J Biol Sci. 2024 Feb;31(2):103920.

3. Laubach J, Richardson P, Anderson K. Multiple myeloma. Annu Rev Med. 2011;62:249–64.

4. Oyajobi BO. Multiple myeloma/hypercalcemia. Arthritis Res Ther. 2007;9:S4.

5. Vakiti A, Padala SA, Hashmi MF, Mewawalla P. Renal Disease in Monoclonal Gammopathies. In: StatPearls [Internet]. Treasure Island (FL): StatPearls Publishing; 2025 [cited 2025 Sept 4]. Available from: http://www.ncbi.nlm.nih.gov/books/NBK499952/

6. Wacka E, Nicikowski J, Jarmuzek P, Zembron-Lacny A. Anemia and Its Connections to Inflammation in Older Adults: A Review. J Clin Med. 2024 Apr 2;13(7):2049.

7. Giorgi PD, Schirò GR, Capitani D, D'Aliberti G, Gallazzi E. Vertebral compression fractures in multiple myeloma: redefining the priorities during the COVID-19 pandemic. Aging Clin Exp Res. 2020;32(7):1203–6.

8. Maura F, Bolli N, Rustad EH, Hultcrantz M, Munshi N, Landgren O. Moving From Cancer Burden to Cancer Genomics for Smoldering Myeloma: A Review. JAMA Oncol. 2020 Mar 1;6(3):425–32.

9. Kyle RA, Rajkumar SV. Monoclonal gammopathy of undetermined significance and smoldering multiple myeloma. Curr Hematol Malig Rep. 2010 Apr;5(2):62–9.

10. Barwick BG, Gupta VA, Vertino PM, Boise LH. Cell of Origin and Genetic Alterations in the Pathogenesis of Multiple Myeloma. Front Immunol. 2019 May 21;10:1121.

11. Lim VY, Zehentmeier S, Fistonich C, Pereira JP. A chemoattractant-guided walk through lymphopoiesis: from hematopoietic stem cells to mature B lymphocytes. Adv Immunol. 2017;134:47–88.

12. Petrilla C, Galloway J, Kudalkar R, Ismael A, Cottini F. Understanding DNA Damage Response and DNA Repair in Multiple Myeloma. Cancers. 2023 Aug 17;15(16):4155.

13. Ni IBP, Ching NC, Meng CK, Zakaria Z. Translocation t(11;14) (q13;q32) and genomic imbalances in multi-ethnic multiple myeloma patients: a Malaysian study. Hematol Rep. 2012 Sept 28;4(3):e19.

14. Kadam Amare P, Nikalje Khasnis S, Hande P, Lele H, Wable N, Kaskar S, et al. Cytogenetic Abnormalities in Multiple Myeloma: Incidence, Prognostic Significance, and Geographic Heterogeneity in Indian and Western Populations. Cytogenet Genome Res. 2023 Aug;162(10):529–40.

15. Sutanto H, Romadhon PZ, Fatmawati VR, Waitupu A, Ansharullah BA, Rachma B, et al. Multiple Myeloma and Precursor Plasma Cell Disorders: From Emerging Driver Mutations to Current and Future Therapeutic Strategies. Hemato. 2025 Sept;6(3):29.

16. Fotiou D, Katodritou E. From Biology to Clinical Practice: The Bone Marrow Microenvironment in Multiple Myeloma. J Clin Med. 2025 Jan 8;14(2):327.

17. Jonsdottir G, Lund SH, Björkholm M, Turesson I, Wahlin A, Mailankody S, et al. Survival in multiple myeloma patients who develop second malignancies: a population-based cohort study. Haematologica. 2016 Apr;101(4):e145–8.

18. Nadeem O, Tai YT, Anderson KC. Immunotherapeutic and Targeted Approaches in Multiple Myeloma. ImmunoTargets Ther. 2020 Oct 14;9:201–15.

19. Gandolfi S, Laubach JP, Hideshima T, Chauhan D, Anderson KC, Richardson PG. The proteasome and proteasome inhibitors in multiple myeloma. Cancer Metastasis Rev. 2017 Dec;36(4):561–84.

20. Dou QP, Zonder JA. Overview of Proteasome Inhibitor-Based Anti-cancer Therapies: Perspective on Bortezomib and Second-Generation Proteasome Inhibitors versus Future Generation Inhibitors of Ubiquitin-Proteasome System. Curr Cancer Drug Targets. 2014;14(6):517–36.

21. Quach H, Ritchie D, Stewart A, Neeson P, Harrison S, Smyth M, et al. Mechanism of action of immunomodulatory drugs (IMiDS) in multiple myeloma. Leukemia. 2010 Jan;24(1):22–32.

22. Lebel E, Nachmias B, Pick M, Gross Even-Zohar N, Gatt ME. Understanding the Bioactivity and Prognostic Implication of Commonly Used Surface Antigens in Multiple Myeloma. J Clin Med. 2022 Jan;11(7):1809.

23. Daratumumab for the Treatment of Multiple Myeloma: A Review of Clinical Applicability and Operational Considerations - Justin R. Arnall, Kathryn T. Maples, R. Donald Harvey, Donald C. Moore, 2022 [Internet]. [cited 2025 Oct 15]. Available from: https://journals.sagepub.com/doi/full/10.1177/10600280211058754?casa_token=OzcIMA95-z8AAAAA%3Avci45l-AxM7cEMm6vVb67-x_4AzHSEbwJAUtbxqZger5tLudMySTX1BJCXxT2UzPBDHxOwIAzJTW

24. Romano A, Storti P, Marchica V, Scandura G, Notarfranchi L, Craviotto L, et al. Mechanisms of Action of the New Antibodies in Use in Multiple Myeloma. Front Oncol. 2021 July 8;11:684561.

25. Wang Y, Sanchez L, Siegel DS, Wang ML. Elotuzumab for the treatment of multiple myeloma. J Hematol OncolJ Hematol Oncol. 2016 July 15;9(1):55.

26. Fulati W, Ma J, Wu M, Qian W, Chen P, Hu Y, et al. Consolidation therapy with autologous stem cell transplantation after remission of induction chemotherapy prolongs the survival of patients with peripheral T-cell lymphoma. Front Immunol. 2024 May 10;15:1382189.

27. Fu Z, Li S, Han S, Shi C, Zhang Y. Antibody drug conjugate: the “biological missile” for targeted cancer therapy. Signal Transduct Target Ther. 2022 Mar 22;7(1):93.

28. Ievoli G. Antibody-drug conjugates charged with unconventional payloads. 2023 [cited 2025 Oct 15]; Available from: https://usiena-air.unisi.it/handle/11365/1233321

29. Doronina SO, Toki BE, Torgov MY, Mendelsohn BA, Cerveny CG, Chace DF, et al. Development of potent monoclonal antibody auristatin conjugates for cancer therapy. Nat Biotechnol. 2003 July;21(7):778–84.

30. Sasso JM, Tenchov R, Bird R, Iyer KA, Ralhan K, Rodriguez Y, et al. The Evolving Landscape of Antibody–Drug Conjugates: In Depth Analysis of Recent Research Progress. Bioconjug Chem. 2023 Nov 15;34(11):1951–2000.

31. Nobari ST, Nojadeh JN, Talebi M. B-cell maturation antigen targeting strategies in multiple myeloma treatment, advantages and disadvantages. J Transl Med. 2022 Feb 10;20(1):82.

32. Farooq AV, Degli Esposti S, Popat R, Thulasi P, Lonial S, Nooka AK, et al. Corneal Epithelial Findings in Patients with Multiple Myeloma Treated with Antibody-Drug Conjugate Belantamab Mafodotin in the Pivotal, Randomized, DREAMM-2 Study. Ophthalmol Ther. 2020 Dec;9(4):889–911.

33. Cogan DG, Kuwabara T. Lipid keratopathy and atheroma. Circulation. 1958 Oct;18(4 Part 1):519–25.

34. Friedman M, Byers SO. EXCESS LIPID LEAKAGE: A PROPERTY OF VERY YOUNG VASCULAR ENDOTHELIUM. Br J Exp Pathol. 1962 Aug;43(4):363–72.

35. Cursiefen C, Hofmann-Rummelt C, Küchle M, Schlötzer-Schrehardt U. Pericyte recruitment in human corneal angiogenesis: an ultrastructural study with clinicopathological correlation. Br J Ophthalmol. 2003 Jan;87(1):101–6.

36. Tabet F, Rye KA. High-density lipoproteins, inflammation and oxidative stress. Clin Sci Lond Engl 1979. 2009 Jan;116(2):87–98.

37. Nazir S, Jankowski V, Bender G, Zewinger S, Rye KA, van der Vorst EPC. Interaction between high-density lipoproteins and inflammation: Function matters more than concentration! Adv Drug Deliv Rev. 2020 Jan 1;159:94–119.

38. Farías MA, Diethelm-Varela B, Navarro AJ, Kalergis AM, González PA. Interplay between Lipid Metabolism, Lipid Droplets, and DNA Virus Infections. Cells. 2022 July 17;11(14):2224.

39. Fan S, Guo J, Nie H, Xiong H, Xia Y. Aberrant Energy Metabolism in Tumors and Potential Therapeutic Targets. Genes Chromosomes Cancer. 2024 Nov;63(11):e70008.

40. Jin Y, Tan Y, Wu J, Ren Z. Lipid droplets: a cellular organelle vital in cancer cells. Cell Death Discov. 2023 July 20;9:254.

41. Fernández LP, Gómez de Cedrón M, Ramírez de Molina A. Alterations of Lipid Metabolism in Cancer: Implications in Prognosis and Treatment. Front Oncol. 2020 Oct 28;10:577420.

42. Song P, Jiang Q, Wu X, Bu L, Xie W, Wei W, et al. Palmitic acid and palmitoylation in cancer: Understanding, insights, and challenges. The Innovation. 2025 Apr 29;6(8):100918.

43. Mortensen MS, Ruiz J, Watts JL. Polyunsaturated Fatty Acids Drive Lipid Peroxidation during Ferroptosis. Cells. 2023 Mar 4;12(5):804.

44. Boyle EM, Davies FE, Leleu X, Morgan GJ. Understanding the multiple biological aspects leading to myeloma. Haematologica. 2014 Apr;99(4):605–12.

45. Chen D, Guo Z, Yao L, Sun Y, Dian Y, Zhao D, et al. Targeting oxidative stress-mediated regulated cell death as a vulnerability in cancer. Redox Biol. 2025 May 19;84:103686.

46. Zhang W, Liu Y, Liao Y, Zhu C, Zou Z. GPX4, ferroptosis, and diseases. Biomed Pharmacother. 2024 May 1;174:116512.

47. Lazaris V, Hatziri A, Symeonidis A, Kypreos KE. The Lipoprotein Transport System in the Pathogenesis of Multiple Myeloma: Advances and Challenges. Front Oncol. 2021 Mar 26;11:638288.

48. Efficacy and safety of single-agent belantamab mafodotin versus pomalidomide plus low-dose dexamethasone in patients with relapsed or refractory multiple myeloma (DREAMM-3): a phase 3, open-label, randomised study - The Lancet Haematology [Internet]. [cited 2025 Oct 16]. Available from: https://www.thelancet.com/journals/lanhae/article/PIIS2352-3026(23)00243-0/abstract

49. Lonial S, Lee HC, Badros A, Trudel S, Nooka AK, Chari A, et al. Belantamab mafodotin for relapsed or refractory multiple myeloma (DREAMM-2): a two-arm, randomised, open-label, phase 2 study. Lancet Oncol. 2020 Feb;21(2):207–21.

50. Popat R, Augustson B, Gironella M, Lee C, Cannell P, Patel N, et al. Results from Arm A of Phase 1/2 DREAMM-6 trial: belantamab mafodotin with lenalidomide plus dexamethasone in patients with relapsed/refractory multiple myeloma. Blood Cancer J. 2024 Oct 21;14(1):184.

51. Tedder B, Bhutani M. Resistance Mechanisms to BCMA Targeting Bispecific Antibodies and CAR T-Cell Therapies in Multiple Myeloma. Cells. 2025 July 15;14(14):1077.

52. Mathias RA, Velkoska E, Didichenko SA, Greene BH, Tan X, Navdaev AV, et al. Apolipoprotein A1 (CSL112) Increases Lecithin-Cholesterol Acyltransferase Levels in HDL Particles and Promotes Reverse Cholesterol Transport. JACC Basic Transl Sci. 2024 Nov 15;10(4):405–18.

53. Panaroni C, Fulzele K, Mori T, Siu KT, Onyewadume C, Maebius A, et al. Multiple myeloma cells induce lipolysis in adipocytes and uptake fatty acids through fatty acid transporter proteins. Blood. 2022 Feb 10;139(6):876–88.

54. Delmas D, Mialhe A, Cotte AK, Connat JL, Bouyer F, Hermetet F, et al. Lipid metabolism in cancer: Exploring phospholipids as potential biomarkers. Biomed Pharmacother. 2025 June 1;187:118095.

55. Wahab A, Rafae A, Mushtaq K, Masood A, Ehsan H, Khakwani M, et al. Ocular Toxicity of Belantamab Mafodotin, an Oncological Perspective of Management in Relapsed and Refractory Multiple Myeloma. Front Oncol. 2021 May 11;11:678634.

56. Walther TC, Farese RV. Lipid Droplets And Cellular Lipid Metabolism. Annu Rev Biochem. 2012;81:687–714.

57. Ackermann T, Shokry E, Deshmukh R, Anand J, Galbraith LCA, Mitchell L, et al. Breast cancer secretes anti-ferroptotic MUFAs and depends on selenoprotein synthesis for metastasis. EMBO Mol Med. 2024 Oct 21;16(11):2749–74.

58. Dixon SJ, Lemberg KM, Lamprecht MR, Skouta R, Zaitsev EM, Gleason CE, et al. Ferroptosis: an iron-dependent form of nonapoptotic cell death. Cell. 2012 May 25;149(5):1060–72.

59. Giallongo C, Tibullo D, Puglisi F, Barbato A, Vicario N, Cambria D, et al. Inhibition of TLR4 Signaling Affects Mitochondrial Fitness and Overcomes Bortezomib Resistance in Myeloma Plasma Cells. Cancers. 2020 July 22;12(8):1999.

60. Tibullo D, Giallongo C, Romano A, Vicario N, Barbato A, Puglisi F, et al. Mitochondrial Functions, Energy Metabolism and Protein Glycosylation are Interconnected Processes Mediating Resistance to Bortezomib in Multiple Myeloma Cells. Biomolecules. 2020 Apr 30;10(5):696.

61. Camiolo G, Barbato A, Giallongo C, Vicario N, Romano A, Parrinello NL, et al. Iron regulates myeloma cell/macrophage interaction and drives resistance to bortezomib. Redox Biol. 2020 Sept;36:101611.

62. Olivares-Vicente M, Herranz-López M. The Interplay Between Oxidative Stress and Lipid Composition in Obesity-Induced Inflammation: Antioxidants as Therapeutic Agents in Metabolic Diseases. Int J Mol Sci. 2025 Sept 2;26(17):8544.

63. Tyurina YY, Shrivastava I, Tyurin VA, Mao G, Dar HH, Watkins S, et al. 'Only a Life Lived for Others Is Worth Living': Redox Signaling by Oxygenated Phospholipids in Cell Fate Decisions. Antioxid Redox Signal. 2018 Nov 1;29(13):1333–58.

64. Zhou Q, Meng Y, Le J, Sun Y, Dian Y, Yao L, et al. Ferroptosis: mechanisms and therapeutic targets. MedComm. 2024 Nov 20;5(12):e70010.

65. Gan B. ACSL4, PUFA, and ferroptosis: new arsenal in anti-tumor immunity. Signal Transduct Target Ther. 2022 Apr 22;7(1):128.

66. Alves F, Lane D, Nguyen TPM, Bush AI, Ayton S. In defence of ferroptosis. Signal Transduct Target Ther. 2025 Jan 3;10:2.

67. Li FJ, Long HZ, Zhou ZW, Luo HY, Xu SG, Gao LC. System Xc -/GSH/GPX4 axis: An important antioxidant system for the ferroptosis in drug-resistant solid tumor therapy. Front Pharmacol. 2022;13:910292.

68. A guide to ferroptosis, the biological rust of cellular membranes - Veeckmans - 2024 - The FEBS Journal - Wiley Online Library [Internet]. [cited 2025 Oct 16]. Available from: https://febs.onlinelibrary.wiley.com/doi/10.1111/febs.16993

69. Giallongo S, Duminuco A, Dulcamare I, Zuppelli T, La Spina E, Scandura G, et al. Engagement of Mesenchymal Stromal Cells in the Remodeling of the Bone Marrow Microenvironment in Hematological Cancers. Biomolecules. 2023 Nov 24;13(12):1701.

70. Kim J, Denu RA, Dollar BA, Escalante LE, Kuether JP, Callander NS, et al. Macrophages and mesenchymal stromal cells support survival and proliferation of multiple myeloma cells. Br J Haematol. 2012 Aug;158(3):336–46.

71. Zheng N, Li F, Huang Q, Huang X, Maj T. Macrophages and macrophage extracellular vesicles confer cancer ferroptosis resistance via PRDX6-mediated mitophagy inhibition. Redox Biol. 2025 Oct 1;86:103826.

6. Figure Credits

1. Fig. 1: F. Maura and P. L. Bergsagel. Molecular Pathogenesis of Multiple Myeloma: Clinical Implications. Hematology/Oncology Clinics 2024 Vol. 38 Issue 2 Pages 267-279 DOI: 10.1016/j.hoc.2023.12.010. https://doi.org/10.1016/j.hoc.2023.12.010.

2. Fig. 2: Raje, N., Mateos, M. V., Iida, S., & Reece, D. (2023). Clinical evidence for immune-based strategies in early-line multiple myeloma: current challenges in decision-making for subsequent therapy. Blood cancer journal, 13(1), 41. https://doi.org/10.1038/s41408-023-00804-y.

3. Fig. 3: https://www.adcreview.com/news/belantamab-mafodotin-receives-priority-review-for-relapsed-or-refractory-multiple-myeloma/

4. Fig. 4: Lazaris V, Hatziri A, Symeonidis A, Kypreos KE. The Lipoprotein Transport System in the Pathogenesis of Multiple Myeloma: Advances and Challenges. Front Oncol. 2021 Mar 26;11:638288.

7. Supplementary data tables

Tab 1A: List of significantly changed proteins in NDMM condition versus HD one. Uniprot ID, gene name, protein name, p-value, and fold change were summarized.

Uniprot ID	Gene name	Protein name	p-Value NDMM/CTRL	Fold Change NDMM/CTRL
P02675	FIBB	Fibrinogen beta chain	1.38E-33	6.80E-10
P02679	FIBG	Fibrinogen gamma chain	1.08E-27	1.11E-09
P02671	FIBA	Fibrinogen alpha chain	7.32E-03	1.22E-02
P63261	ACTG	Actin, cytoplasmic 2	2.20E-05	0.07
P69905	HBA	Haemoglobin subunit alpha	4.49E-04	0.30
P68871	HBB	Haemoglobin subunit beta	2.25E-03	0.40
P01876	IGHA1	Immunoglobulin heavy constant alpha 1	2.92E-03	0.43
P02751	FINC	Fibronectin	7.90E-03	0.47
P0DOY2	IGLC2	Immunoglobulin lambda constant 2	4.09E-04	0.49
P02749	APOH	Beta-2-glycoprotein 1	6.18E-06	0.52
P02765	FETUA	Alpha-2-HS-glycoprotein	1.86E-02	0.70
P02768	ALBU	Albumin	4.59E-03	0.85
P01009	A1AT	Alpha-1-antitrypsin	8.97E-04	1.58
P02790	HEMO	Hemopexin	9.63E-03	1.68
P01011	AACT	Alpha-1-antichymotrypsin	1.88E-02	1.83
P04196	HRG	Histidine-rich glycoprotein	3.78E-03	1.89
P02652	APOA2	Apolipoprotein A-II	5.36E-04	2.11
P02655	APOC2	Apolipoprotein C-II	3.16E-04	2.29
P00450	CERU	Ceruloplasmin	1.26E-02	2.34
P02647	APOA1	Apolipoprotein A-I	1.73E-04	2.38
P06727	APOA4	Apolipoprotein A-IV	5.41E-03	2.57
P0DOX5	IGG1	Immunoglobulin gamma-1 heavy chain	9.53E-03	2.87
P04114	APOB	Apolipoprotein B-100	1.50E-04	3.47
P02750	A2GL	Leucine-rich alpha-2-glycoprotein	3.57E-03	5.90
P36955	PEDF	Pigment epithelium-derived factor	1.92E-03	14355963.00
P51884	LUM	Lumican	1.91E-03	18169441.46
P0DOX7	IGK	Immunoglobulin kappa light chain	9.58E-03	134086532.10

Tab 2B: List of significantly changed proteins in RRMM condition versus HD one. Uniprot ID, gene name, protein name, p-value, and fold change were summarized

Uniprot ID	Gene name	Protein name	p-Value RRMM/CTRL	Fold Change RRMM/CTRL
P02675	FIBB	Fibrinogen beta chain	6.51E-36	6.80E-10
P02679	FIBG	Fibrinogen gamma chain	1.26E-29	1.11E-09
P01591	IGJ	Immunoglobulin J chain	5.03E-20	1.37E-08
P63261	ACTG	Actin, cytoplasmic 2	1.76E-31	1.38E-08
O43866	CD5L	CD5 antigen-like	9.52E-05	5.81E-08
P0DOX2	IGA2	Immunoglobulin alpha-2 heavy chain	9.54E-05	7.29E-08
P02671	FIBA	Fibrinogen alpha chain	8.66E-11	7.07E-03
P01876	IGHA1	Immunoglobulin heavy constant alpha 1	3.04E-07	0.07
P69905	HBA	Haemoglobin subunit alpha	2.12E-02	0.08
P01859	IGHG2	Immunoglobulin heavy constant gamma 2	2.31E-02	0.11
P68871	HBB	Haemoglobin subunit beta	4.96E-08	0.13
P01871	IGHM	Immunoglobulin heavy constant mu	1.55E-07	0.21
P02751	FINC	Fibronectin	8.95E-04	0.37
P02749	APOH	Beta-2-glycoprotein 1	2.94E-07	0.46
P06396	GELS	Gelsolin	2.34E-03	0.49
P04264	K2C1	Keratin, type II cytoskeletal 1	9.83E-03	0.65
P02765	FETUA	Alpha-2-HS-glycoprotein	3.65E-02	0.71
P08697	A2AP	Alpha-2-antiplasmin	2.59E-03	0.78
P02768	ALBU	Albumin	2.15E-04	0.78
P02774	VTDB	Vitamin D-binding protein	2.80E-02	0.80
P27169	PON1	Serum paraoxonase/arylesterase 1	1.88E-02	0.89
P00734	THRB	Prothrombin	7.30E-03	1.21
P10909	CLUS	Clusterin	1.56E-02	1.25
P04217	A1BG	Alpha-1B-glycoprotein	3.21E-02	1.29
Q14624	ITIH4	Inter-alpha-trypsin inhibitor heavy chain H4	6.92E-03	1.30
P01009	A1AT	Alpha-1-antitrypsin	3.13E-04	1.42
P0DOX8	IGL1	Immunoglobulin lambda-1 light chain	1.81E-04	1.42
P19652	A1AG2	Alpha-1-acid glycoprotein 2	3.70E-02	1.43
P19823	ITIH2	Inter-alpha-trypsin inhibitor heavy chain H2	2.64E-02	1.52
P02790	HEMO	Hemopexin	1.72E-03	1.55
P02763	A1AG1	Alpha-1-acid glycoprotein 1	4.30E-03	1.91
P01019	ANGT	Angiotensinogen	1.34E-04	1.91
P00450	CERU	Ceruloplasmin	2.35E-02	2.09
P02652	APOA2	Apolipoprotein A-II	2.45E-04	2.11
P02655	APOC2	Apolipoprotein C-II	3.73E-07	2.21

P01011	AACT	Alpha-1-antichymotrypsin	7.48E-04	2.55
P02647	APOA1	Apolipoprotein A-I	3.82E-06	2.76
P02649	APOE	Apolipoprotein E	2.21E-02	2.83
P06727	APOA4	Apolipoprotein A-IV	9.43E-05	3.18
P02656	APOC3	Apolipoprotein C-III	8.39E-06	3.50
P02753	RET4	Retinol-binding protein 4	3.57E-05	3.95
P04114	APOB	Apolipoprotein B-100	7.37E-06	4.61
P01861	IGHG4	Immunoglobulin heavy constant gamma 4	3.16E-02	5.66
P02750	A2GL	Leucine-rich alpha-2-glycoprotein	1.56E-03	9.51
P0DJI8	SAA1	Serum amyloid A-1 protein	0.04	13.01
P36955	PEDF	Pigment epithelium-derived factor	8.87E-04	20128553.15
P02654	APOC1	Apolipoprotein C-I	8.87E-04	22110508.86

8. Supplementary figures

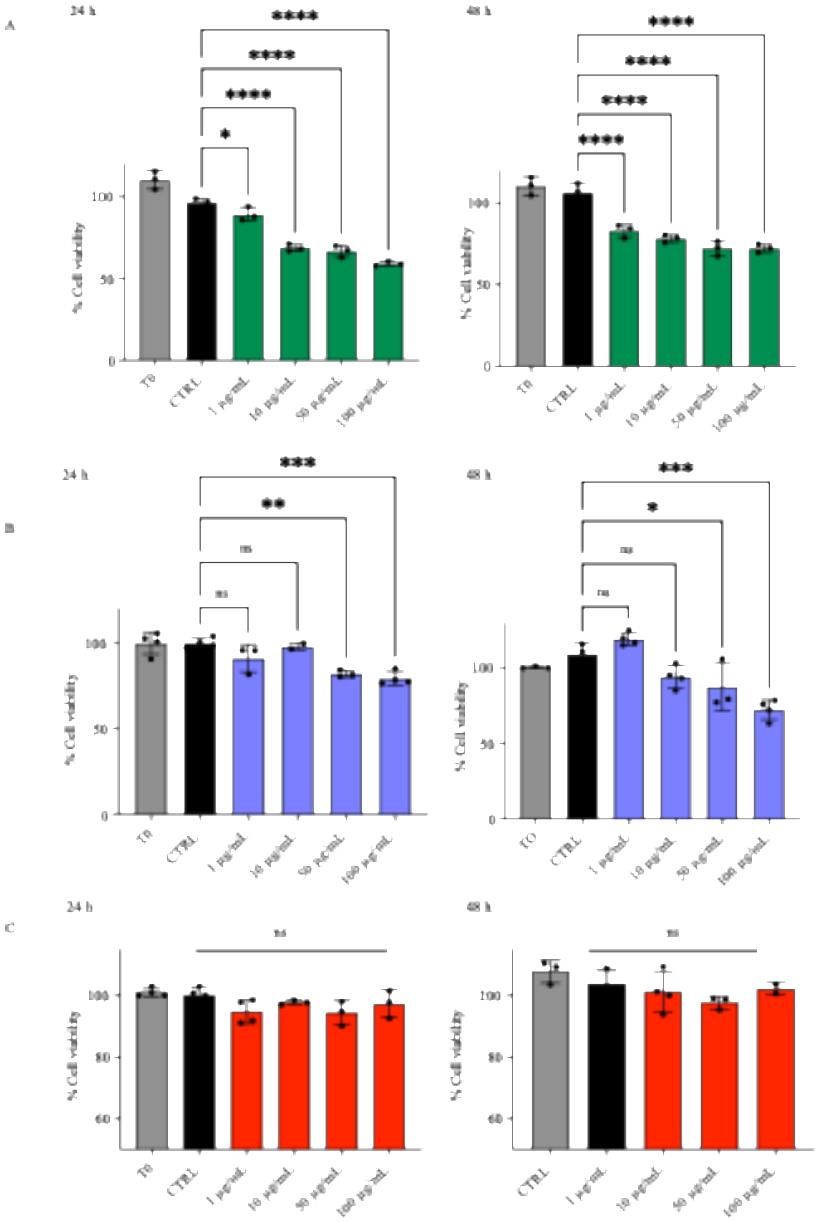

Supplementary Fig. 1 - Dose–response curve of BeMa in MM cells. U266, NCI-H929, and OPM2 cells were treated for 48 h with increasing concentrations of BeMa ranging from 1 to 100 µg/mL, and cell viability was assessed by XTT assay.